Applied Physics Letters

Silicon integrated terahertz quantum cascade ring laser frequency comb

Cite as: Appl. Phys. Lett. **120**, 091106 (2022); https://doi.org/10.1063/5.0078749
Submitted: 15 November 2021 • Accepted: 23 February 2022 • Published Online: 01 March 2022

M. Jaidl, N. Opačak, M. A. Kainz, et al.

Applied Physics Letters ARTICLE scitation.org/journal/apl

Silicon integrated terahertz quantum cascade ring laser frequency comb

Cite as: Appl. Phys. Lett. **120**, 091106 (2022); doi: 10.1063/5.0078749
Submitted: 15 November 2021 · Accepted: 23 February 2022 ·
Published Online: 1 March 2022

M. Jaidl,[1,2,a] N. Opačak,[3] M. A. Kainz,[1,2] D. Theiner,[1,2] B. Limbacher,[1,2] M. Beiser,[2,3] M. Giparakis,[2,3] A. M. Andrews,[2,3] G. Strasser,[2,3] B. Schwarz,[2,3] J. Darmo,[1,2] and K. Unterrainer[1,2]

AFFILIATIONS

[1]Photonics Institute, TU Wien, Gusshausstrasse 27-29, 1040 Wien, Austria
[2]Center for Micro- and Nanostructures, TU Wien, Gusshausstrasse 25a, 1040 Wien, Austria
[3]Institute of Solid State Electronics, TU Wien, Gusshausstrasse 25a, 1040 Wien, Austria

[a)]Author to whom correspondence should be addressed: michael.jaidl@tuwien.ac.at

ABSTRACT

We demonstrate terahertz quantum cascade lasers realized in "ideal" ring resonators without discontinuities from, e.g., contacting pads. We realize this by mounting rings episide-down on a silicon substrate by a die-bonding technique. This technique allows one to realize ideal conditions for optical confinement as well as heat dissipation and provides the basis for future Si integrated THz devices. The lasers emit light around 3.8 THz and show much reduced threshold current densities. When operated in continuous-wave operation, frequency comb formation with a spectral bandwidth of 70 GHz is observed. Frequency comb operation is indicated by a narrow beat note signal at 8.55 GHz with a signal-to-noise ratio up to 40 dB. The experimentally measured spectral behavior of ring devices is described accurately by the results obtained from numerical simulations based on the Maxwell–Bloch formalism.

In recent years, reliable optical frequency comb[1] sources have been realized in the mid-infrared and terahertz (THz) region by using quantum cascade lasers (QCLs).[2–5] These electrically driven, on-chip sources of light provide simultaneously high output power and compact design, making them ideal candidates for portable high-precision spectroscopic applications. When it comes to choosing the laser resonator geometry, ring resonators outperform commonly used ridge type waveguides supporting Fabry–Pérot (FP) modes in several aspects. Ring resonators support whispering gallery modes (WGMs),[6] which are guided by total internal reflection on the outer perimeter of the resonator. Hence, the radiation losses are comparatively lower in ring resonators. This leads to a lower lasing threshold and driving currents, which results in a lower heat dissipation in the devices. The latter is especially essential for continuous-wave high-performance laser operation. The lower optical loss of ring resonators compared to that of FP resonators causes higher intracavity intensities, which leads to stronger saturation of the gain[7] and increased nonlinear effects. The interplay of these increased nonlinearities and the dispersion[8] should, therefore, favor comb formation more in ring cavity geometries.[9] From an experimental point of view, in FP resonators, a complex dispersion compensation geometry[3] or a carefully designed gain shape of the active material[4,5] was used to achieve the comb formation. Moreover, multimode operation in FP resonators is primarily triggered by the effect of spatial hole burning (SHB) due to the standing wave pattern formed by the opposite propagating components of the laser light inside the resonator. The influence of SHB can be switched to ring resonators by implementing defects that break the rotational symmetry of the resonator geometry and provide a reflection point.[10] However, by fabricating defect-free ring geometries, SHB with its negative side effects, such as gain compression, linewidth broadening, and mode-hopping,[11–13] can be avoided.

THz QCLs are usually processed on a GaAs or InP substrate and afterwards mounted onto a coldfinger for operation. However, it would open up countless possibilities if these devices could be integrated on prepared chips containing waveguides, detectors, or modulators. It would be especially attractive to combine THz QCLs with the well-established silicon photonics.[14,15] By mounting the lasers onto pre-processed silicon chips, arbitrary THz circuit configurations such as source–waveguide–detector systems or designs with fast modulators become possible, as waveguides' plasmonic or low loss Si waveguides[16] can be employed. We think that this technique can also lead to lab-on-a-chip systems, e.g., for gas sensing.

In this work, we report on defect-free ring-shaped THz QCLs. We use a die-bonding technique to realize episide-down mounting onto a Si chip, enabling the use of very thin widths of the ring waveguide without the necessity of implementing bonding pads for electrical contacting. This allows the realization of ideal, defectless ring resonators, where the main mechanism responsible for multimode instability is the phase turbulence.[17] This mounting technique provides an increased optical confinement in the waveguide and better heat extraction, which leads to a lower active region temperature.[18,19] These two improvements result in a decreased threshold current density of the lasers. When combined with proper heat extraction, these are especially important for continuous-wave operation, which is a prerequisite for free-running comb formation. In the episide-down mounted rings without contacting pad discontinuities, frequency combs are formed, which are well explained by a theoretical model.[17]

The QCL active region used in this study is based on a single-stack, three-well, longitudinal optical (LO)-phonon depopulation design in the GaAs/AlGaAs-material system, which is also used in Ref. 9. It consists of 345 periods and has a total thickness of 15 m. The active region is processed into ring-shaped, double-metal waveguides (DMWGs) to provide high confinement and low optical losses. An additional center pillar consisting of the active region, which functions as a stabilization and heat transfer platform, remains in the middle of the ring. The distance between the ring and the pillar is 150 m. Due to the narrow width of the devices, a direct wire bonding technique for electrical contacting is not possible. Therefore, the rings processed on the chip are cleaved into single ring chips. A single ring is then flip-chip bonded onto the Ti/Au-pads (10 nm/1.5 m) of a Si chip by utilizing a sub-micron die-bonder (Finetech Fineplacer lambda). Protruding bridges of the Ti/Au-pads and the bottom of the ring substrate are used for electrical contacting. Note that the Ti/Au-pad for the center pillar is electrically disconnected from the ring pad, which ensures that the pillar is not pumped during the operation of the ring device. This episide-down mounting technique also leads to an improved heat management due to the additional heat sink connections. A sketch of the episide-down fabrication steps is shown in Fig. 1(a). In Fig. 1(b), the simulated field distribution in a segment of the ring waveguide computed by a commercial finite element solver is shown. The increased optical confinement becomes clear when comparing it to simulation of the episide-up rings in Ref. 9. The mode in the episide-down mounted ring is strongly confined inside the waveguide and does not leak out of the cavity as seen in the episide-up counterpart. This change of the mode profile is caused by the sandwich structure of the episide-down mounted ring, which changes the boundary conditions in the vicinity of the rim edge. The contacting structure on the Si substrate, which creates this sandwich structure, is highlighted in dark green in Fig. 1(b).

The silicon chip with the ring devices on top is indium soldered to a copper plate, which is mounted onto the coldfinger of a He flow cryostat. Due to the DMWG geometry of the devices, the light is emitting from the rim edges of the rings. Therefore, only a fraction of the emitted light is collected by a parabolic mirror and guided into a Fourier transform infrared spectrometer (FTIR), where the spectra are recorded with a resolution of 2.25 GHz. For the power measurement of the laser light, a thermopile detector is placed in front of the laser chip in the horizontal plane of the ring. This thermopile detector also measures only a fraction of the emitted light since the light is emitted from the rim edge throughout the whole circumference of the device. The electrical beat note measurement is enabled through a semi-rigid RF cable, which is installed in parallel to the DC bias lines. The RF cable is plugged to a signal analyzer via a DC-block element. A source-measure-unit Keithley 2602 is used to bias the devices. All measurements are performed in continuous-wave operation.

In Fig. 2(a), the performance of the episide-down mounted ring device with a waveguide width of 15 μm and a diameter of 2 mm at a heat sink temperature of 13 K is shown. The current–voltage characteristics exhibit alignment at the design voltage and no indication of an increased contact resistance proving the reliability of the episide-down mounting. The ring-shaped QCL has a remarkably reduced threshold current of 150 A/cm^2. Compared to the other devices fabricated on the very same active region, the threshold current density is reduced by 40%.[9] This reduction is due to the high confinement of the modes and improved heat extraction caused by the ring-shaped waveguide and the episide-down mounting technique. The ideal ring geometry without waveguide discontinuities also minimizes the mode scattering, which is experimentally manifested in a reduced output

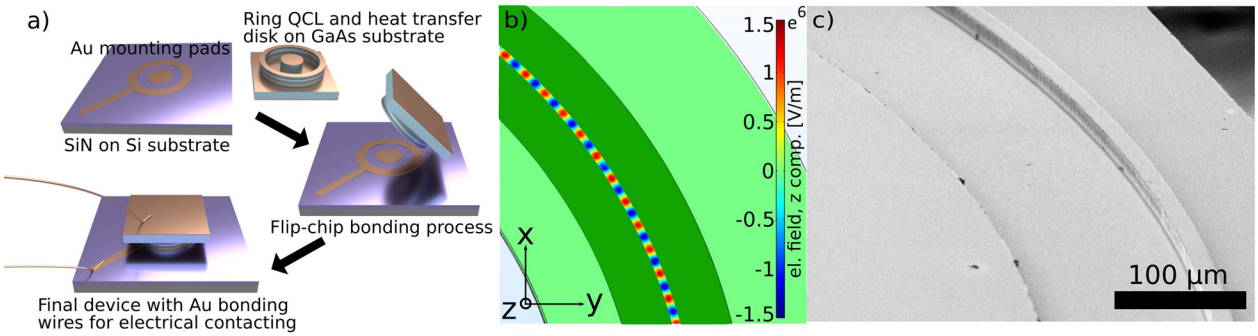

FIG. 1. (a) Fabrication process of the episide-down mounted THz quantum cascade ring lasers. The ring and the pillar are fabricated by a standard process for double-metal waveguides. Single ring chips are then flip-chip bonded onto the Ti/Au-pads of a Si chip. Contacting bridges and the backside of the device substrate are used for electrical contacting. (b) Eigenmode simulation (an electric field in the z-direction) of the ring device using a commercial finite element solver (COMSOL 5.5). The contacting structure on the Si substrate creating the sandwich structure is highlighted in dark green. (c) Scanning electron microscopy (SEM) image of a fabricated ring and heat transfer pillar section.

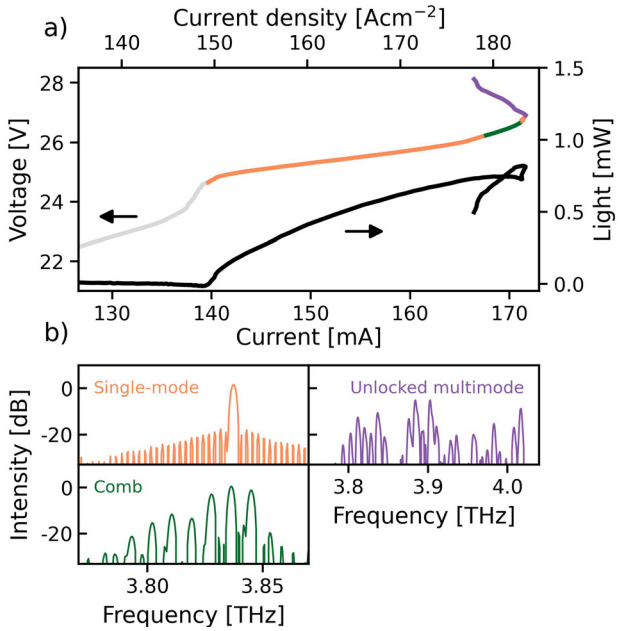

FIG. 2. Emission regimes of the THz quantum cascade ring laser in continuous-wave operation at a heat sink temperature of 13 K. (a) DC light–current–voltage (LIV) measurement in the dynamic range of the ring laser. The ring devices exhibit three different emission regimes, which are colored on the I–V-curve. The devices start lasing the single-mode at the threshold current of 140 mA. They operate in the comb regime between 167 and 172 mA, which collapse to the single-mode again with increasing driving current. The multimode regime is entered only in constant voltage operation, which is active after the second single-mode regime. (b) Corresponding spectra of the three emission regimes.

power. The supporting center pillar in the middle of the ring provides additional heat transfer, and the heat extraction is improved. This leads to a maximum operating temperature of 60 K, which exceeds the episide-up mounted rings by 10 K. The robustness of the devices is shown by the fact that even cooling down to 10 K does not lead to debonding of the mounted laser chip in spite of GaAs and Si having different coefficients of thermal expansion. These results demonstrate clearly the potential of the episide-down mounting on Si substrates: Our approach paves the road toward integration of THz QCLs with waveguides and other devices on a single Si chip and at the same time improves the performance of the lasers mounted in that way.

The devices exhibit three different emission regimes, which can be localized on the current–voltage (I–V) curve [Fig. 2(a)]. In the first regime, at driving currents above the threshold current of 140 mA, the lasers operate in the single-mode. By increasing the driving current, the single-mode regime transitions into the comb regime in the current range between 167 and 172 mA, resulting in a mode spectrum with eight equally spaced modes covering a bandwidth of 70 GHz and an electrically detectable, stable beat note signal. A further increase in the driving current results in collapse of the comb state to single-mode emission again. In constant current operation, the devices stop lasing at 174 mA. When driving the lasers in constant voltage operation, after the second single-mode regime, the negative differential resistance region is entered, and the devices show multimode emission, where the modes are still equally spaced; however, some modes are missing, and no beat note signal is detected. A corresponding spectrum of each emission regime is shown in Fig. 2(b). In the comb region, a single beat note signal with a signal-to-noise ratio (S/N) up to 40 dB is detected. The beatnote frequency is shifting toward lower values with increasing driving voltage (Fig. 3) due to the temperature dependence of the effective refractive index of the active medium. This is explained by the elevated temperature in the waveguide with increasing driving current.[20]

Compared to the recently reported comb formation in ring devices,[9] which exhibit a comb spectrum organized in four separated lobes, the ring devices in this study show a single-lobed spectrum without any spectral holes. While the previously published ring devices contain attached contacting pads, which implement defects in the ring geometry, the devices in this study are defect-free. To shine some light on the actual comb formation in defect-free ring cavities in the THz region, we perform numerical simulations based on the Maxwell–Bloch formalism.[17,21] The multimode instability in the ring resonators is caused by the interplay of dispersion and large optical nonlinearities. The latter is induced by the asymmetrical gain-shape of the active medium, thanks to the ultrafast carrier lifetimes.[7] In our model, the asymmetric gain is implemented using the linewidth enhancement factor (LEF) α. For THz QCLs, longer upper state lifetimes have been reported,[22,23] and the value of the LEF should, in principle, be larger than in the mid-IR QCLs designs[17,24] since the gain shape is highly asymmetric and often consisted of multiple transitions.[25] Figure 4(a) shows simulation of a fundamental frequency comb state using a LEF of $\alpha = 1.6$

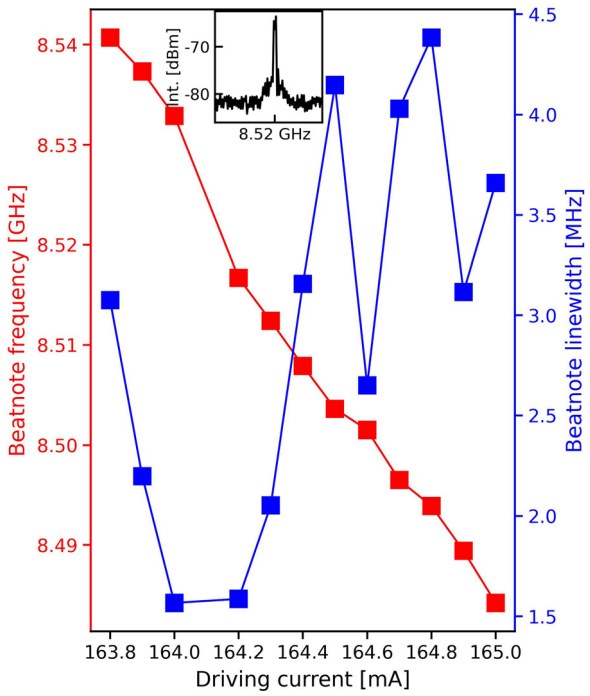

FIG. 3. Intermode beat note frequency and linewidth as a function of the driving current. As the effective refractive index of the ring devices is temperature dependent, the beat note frequency shifts toward lower frequencies due to elevated heat dissipation with increasing driving current. The inset shows the detected beat note signal at a driving current of 164.2 mA.

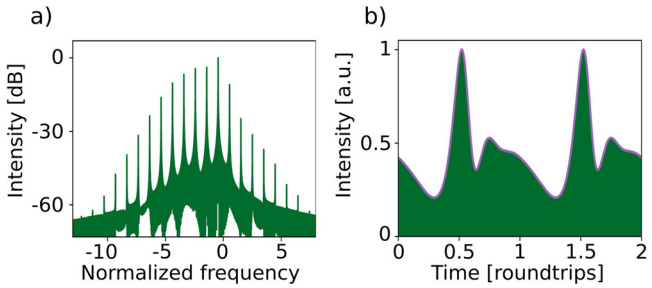

FIG. 4. Numerical simulation of a defect-free ring cavity QCL using the LEF of $\alpha = 1.6$. (a) The power spectrum of the laser intensity over two roundtrips, showing a fundamental frequency comb. In order to reach a stationary state, numerical simulations have been run for 100 000 roundtrips. (b) The time trace of the laser intensity shows high-contrast amplitude modulations on a continuous background.

and an upper-state lifetime of 20 ps (for details of modeling, see the supplementary material of Ref. 9). The simulated data are in good agreement with the experimentally measured spectrum. The time trace of the laser intensity [Fig. 4(b)] shows a high-contrast amplitude modulation on a continuous background. The comb state has this characteristic intensity shape over one round trip and can be achieved within a range of LEF values between 1.3 and 1.7.

In conclusion, we demonstrated the realization of defect-free ring-shaped THz QCLs mounted episide-down onto a Si chip by using a die-bonding technique. The ring lasers exhibit a reduced threshold current density by 40%, compared to other waveguide geometries processed on the same material and show comb formation induced by phase turbulence. Our devices demonstrate self-starting frequency comb operation without a need for any external components or dispersion compensation schemes. The comb regime exhibits eight equidistant modes covering a bandwidth of 70 GHz and a single, temperature dependent beat note signal around 8.55 GHz with a S/N up to 40 dB. The measurement data are in very good agreement with the results obtained from numerical simulations based on the Maxwell–Bloch formalism. Furthermore, the employed die-bonding technique gives opportunities for many other integrated on-chip applications. Due to the building block system of this technique, arbitrary waveguide geometries together with light sources and detectors[26] made of different materials can be combined creating a compact lab-on-a-chip. These results are also promising when it comes to pattern formation in ring resonators. Different emission regimes with one-lobed spectra and separated spectral lobes that are shown in a recent study[9] and this work have been reported in passive microresonators, where the mode evolution eventually leads to the formation of a dissipative Kerr soliton.[27] Recently, it was demonstrated that this kind of soliton is not only restricted to passive media, but can also appear in active electrically pumped media as well. This was achieved in ring-shaped QCLs that emit in the mid-infrared (mid-IR) spectral region, and soliton formation was achieved through dispersion engineering by modifying the ring waveguide width.[28] Due to the similarity of mid-IR QCLs and THz QCLs, dissipative Kerr soliton formation should be feasible in our ring-shaped THz QCLs by employing the same dispersion engineering method.

The authors acknowledge financial support from the Austrian Science Fund FWF (Nos. DK Solids4Fun W1243 and DiPQCL P30709-N27). The authors acknowledge TU Wien Bibliothek for financial support through its Open Access Funding Programme. N.O. and B.S. acknowledge funding from the European Research Council (ERC) under the European Union's Horizon 2020 research and innovation programme (Grant Agreement No. 853014). A.M.A. acknowledges funding through COMTERA, a program under the auspices of ERA.NET RUS PLUS (No. FFG 849614) and AFOSR (No. FA9550-17-1-0340).

AUTHOR DECLARATIONS

Conflict of Interest

The authors have no conflicts to disclose.

DATA AVAILABILITY

The data that support the findings of this study are available from the corresponding author upon reasonable request.

REFERENCES

[1]T. Udem, R. Holzwarth, and T. W. Hänsch, "Optical frequency metrology," Nature **416**, 233–237 (2002).
[2]A. Hugi, G. Villares, S. Blaser, H. C. Liu, and J. Faist, "Mid-infrared frequency comb based on a quantum cascade laser," Nature **492**, 229–233 (2012).
[3]D. Burghoff, T.-Y. Kao, N. Han, C. W. I. Chan, X. Cai, Y. Yang, D. J. Hayton, J.-R. Gao, J. L. Reno, and Q. Hu, "Terahertz laser frequency combs," Nat. Photonics **8**, 462–467 (2014).
[4]M. Rösch, G. Scalari, M. Beck, and J. Faist, "Octave-spanning semiconductor laser," Nat. Photonics **9**, 42–47 (2015).
[5]A. Forrer, M. Franckié, D. Stark, T. Olariu, M. Beck, J. Faist, and G. Scalari, "Photon-driven broadband emission and frequency comb RF injection locking in THz quantum cascade lasers," ACS Photonics **7**, 784–791 (2020).
[6]A. B. Matsko and V. S. Ilchenko, "Optical resonators with whispering-gallery modes—Part I: Basics," IEEE J. Sel. Top. Quantum Electron. **12**, 3–14 (2006).
[7]N. Opačak, S. D. Cin, J. Hillbrand, and B. Schwarz, "Frequency comb generation by Bloch gain induced giant Kerr nonlinearity," Phys. Rev. Lett. **127**, 093902 (2021).
[8]M. Beiser, N. Opačak, J. Hillbrand, G. Strasser, and B. Schwarz, "Engineering the spectral bandwidth of quantum cascade laser frequency combs," Opt. Lett. **46**, 3416–3419 (2021).
[9]M. Jaidl, N. Opačak, M. A. Kainz, S. Schönhuber, D. Theiner, B. Limbacher, M. Beiser, M. Giparakis, A. M. Andrews, G. Strasser, B. Schwarz, J. Darmo, and K. Unterrainer, "Comb operation in terahertz quantum cascade ring lasers," Optica **8**, 780–787 (2021).
[10]D. Kazakov, N. Opačak, M. Beiser, A. Belyanin, B. Schwarz, M. Piccardo, and F. Capasso, "Defect-engineered ring laser harmonic frequency combs," Optica **8**, 1277–1280 (2021).
[11]M. Aoki, K. Uomi, T. Tsuchiya, S. Sasaki, M. Okai, and N. Chinone, "Quantum size effect on longitudinal spatial hole burning in MQW lambda/4-shifted DFB lasers," IEEE J. Quantum Electron. **27**, 1782–1789 (1991).
[12]M. G. Davis and R. F. O'Dowd, "A transfer matrix method based large-signal dynamic model for multielectrode DFB lasers," IEEE J. Quantum Electron. **30**, 2458–2466 (1994).
[13]T. Yamanaka, S. Seki, and K. Yokoyama, "Numerical analysis of static wavelength shift for DFB lasers with longitudinal mode spatial hole burning," IEEE Photonics Technol. Lett. **3**, 610–612 (1991).
[14]A. Spott, J. Peters, M. L. Davenport, E. J. Stanton, C. D. Merritt, W. W. Bewley, I. Vurgaftman, C. S. Kim, J. R. Meyer, J. Kirch, L. J. Mawst, D. Botez, and J. E. Bowers, "Quantum cascade laser on silicon," Optica **3**, 545–551 (2016).
[15]A. Spott, E. J. Stanton, N. Volet, J. D. Peters, J. R. Meyer, and J. E. Bowers, "Heterogeneous integration for mid-infrared silicon photonics," IEEE J. Sel. Top. Quantum Electron. **23**, 1–10 (2017).

[16]K. Tsuruda, M. Fujita, and T. Nagatsuma, "Extremely low-loss terahertz waveguide based on silicon photonic-crystal slab," Opt. Express **23**, 31977–31990 (2015).
[17]M. Piccardo, B. Schwarz, D. Kazakov, M. Beiser, N. Opačak, Y. Wang, S. Jha, J. Hillbrand, M. Tamagnone, W. T. Chen, A. Y. Zhu, L. L. Columbo, A. Belyanin, and F. Capasso, "Frequency combs induced by phase turbulence," Nature **582**, 360–364 (2020).
[18]O. Krüger, S. Kreutzmann, D. Prasai, M. Wienold, R. Sharma, W. Pittroff, L. Weixelbaum, W. John, K. Biermann, L. Schrottke, F. Schnieder, G. Erbert, H. T. Grahn, and G. Tränkle, "Epitaxial-side mounting of terahertz quantum-cascade lasers for improved heat management," IEEE Photonics Technol. Lett. **25**, 1570–1573 (2013).
[19]Y.-Y. Li, J.-Q. Liu, F.-Q. Liu, J.-C. Zhang, S.-Q. Zhai, N. Zhuo, L.-J. Wang, S.-M. Liu, and Z.-G. Wang, "High power-efficiency terahertz quantum cascade laser," Chin. Phys. B **25**, 084206 (2016).
[20]B. Meng, M. Singleton, M. Shahmohammadi, F. Kapsalidis, R. Wang, M. Beck, and J. Faist, "Mid-infrared frequency comb from a ring quantum cascade laser," Optica **7**, 162–167 (2020).
[21]N. Opačak and B. Schwarz, "Theory of frequency-modulated combs in lasers with spatial hole burning, dispersion, and Kerr nonlinearity," Phys. Rev. Lett. **123**, 243902 (2019).
[22]D. R. Bacon, J. R. Freeman, R. A. Mohandas, L. Li, E. H. Linfield, A. G. Davies, and P. Dean, "Gain recovery time in a terahertz quantum cascade laser," Appl. Phys. Lett. **108**, 081104 (2016).
[23]C. G. Derntl, G. Scalari, D. Bachmann, M. Beck, J. Faist, K. Unterrainer, and J. Darmo, "Gain dynamics in a heterogeneous terahertz quantum cascade laser," Appl. Phys. Lett. **113**, 181102 (2018).
[24]R. P. Green, J.-H. Xu, L. Mahler, A. Tredicucci, F. Beltram, G. Giuliani, H. E. Beere, and D. A. Ritchie, "Linewidth enhancement factor of terahertz quantum cascade lasers," Appl. Phys. Lett. **92**, 071106 (2008).
[25]M. A. Kainz, S. Schönhuber, B. Limbacher, A. M. Andrews, H. Detz, G. Strasser, G. Bastard, and K. Unterrainer, "Color switching of a terahertz quantum cascade laser," Appl. Phys. Lett. **114**, 191104 (2019).
[26]P. Micheletti, J. Faist, T. Olariu, U. Senica, M. Beck, and G. Scalari, "Regenerative terahertz quantum detectors," APL Photonics **6**, 106102 (2021).
[27]T. J. Kippenberg, A. L. Gaeta, M. Lipson, and M. L. Gorodetsky, "Dissipative Kerr solitons in optical microresonators," Science **361**, eaan8083 (2018).
[28]B. Meng, M. Singleton, J. Hillbrand, M. Franckié, M. Beck, and J. Faist, "Dissipative Kerr solitons in semiconductor ring lasers," Nat. Photonics **16**, 142–146 (2022).